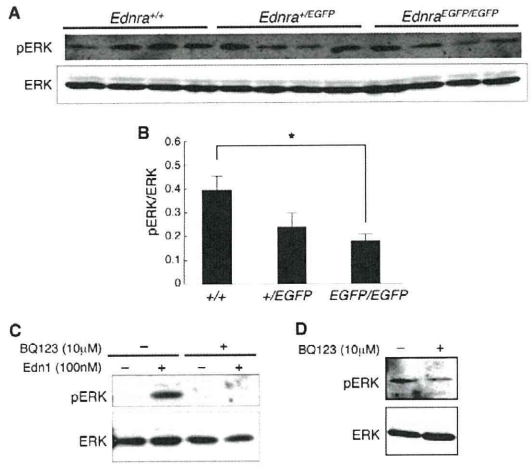

Fig. 7. Analysis of ERK phosphorylation. (**A**) Western blot of individual hearts excised from E9.5 wild-type, *Ednra*$^{+/EGFP}$ and *Ednra*$^{EGFP/EGFP}$ embryos using antibodies to phosphorylated (pERK) and total ERK1/2 (ERK). (**B**) Quantification of the ratio of phosphorylated to total ERK protein levels in A, normalized to control (wild-type) samples (n=5 per group). Data are presented as mean±s.e.m. *P<0.05. (**C**) Edn1 stimulates ERK phosphorylation in isolated E9.5 hearts. Edn1-induced ERK phosphorylation is completely abolished by the Ednra antagonist BQ123. (**D**) BQ123 downregulates basal ERK phosphorylation in isolated E9.5 hearts.

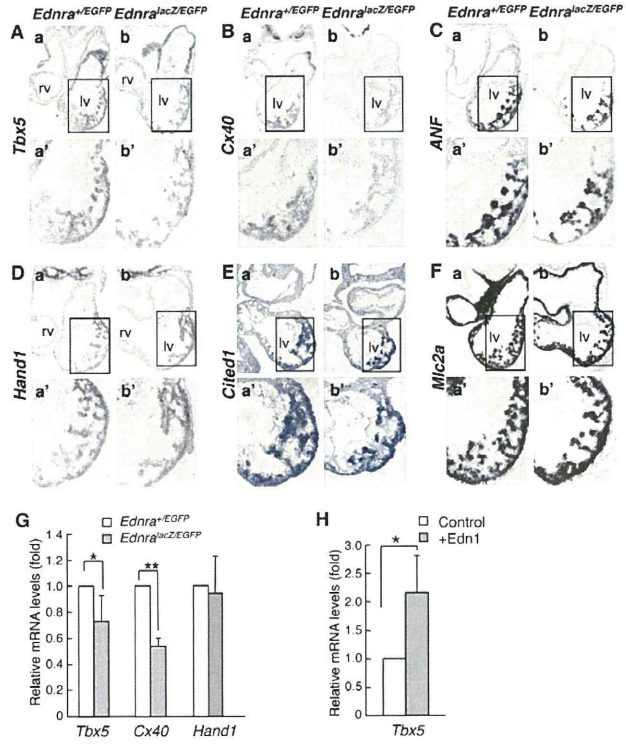

Fig. 8. Gene expression analysis of E9.5 *Ednra*-null hearts. (**A-F**) In situ hybridization of *Ednra*$^{+/EGFP}$ (a,a′) and *Ednra*$^{lacZ/EGFP}$ (b,b′) hearts for *Tbx5* (A), *Cx40* (B), *ANF* (C), *Hand1* (D), *Cited1* (E) and *Mlc2a* (F). a′ and b′ are magnifications of the regions indicated in a and b, respectively. lv, left ventricle; rv, right ventricle. (**G**,**H**) Real-time RT-PCR analysis. (G) *Tbx5* and *Cx40*, but not *Hand1*, expression levels are lower in *Ednra*$^{lacZ/EGFP}$ hearts than in *Ednra*$^{+/EGFP}$ hearts (n=5 per group). (H) In E9.5 wild-type ventricles, *Tbx5* expression is upregulated by stimulation with 100 nM Edn1 for 24 hours (n=4 per group). Data are presented as mean±s.e.m. *P<0.05, **P<0.01.

DISCUSSION

Regionalization of the first heart field and contribution to chamber formation

Here, we identified an *Ednra-lacZ/EGFP*-expressing cell population that is first detected in the cardiac crescent. At the early heart tube-forming stage, these cells are present in the ventral inflow region. Subsequently, dye-labeling experiments indicate that they move upward along the outer curvature between the 6/7-somite and 9/10-somite stages. This timing corresponds to the start of looping just after the formation of the linear heart tube (Abu-Issa and Kirby, 2007), indicating that the linear heart tube is mainly composed of *Ednra*-negative cells and that the *Ednra*-positive cells are recruited into the looping heart tube. This upward cell movement was confirmed and was shown to be specific for cells in the inflow region by dye-labeling and transplantation experiments. These findings suggest that *Ednra*-positive cells arising from the crescent-forming first heart field are a distinct subpopulation and contribute to chamber formation in a manner different from that of the early tube-forming cells.

de la Cruz and colleagues have performed extensive in vivo labeling experiments in the chick and showed that the inflow region between the interventricular grooves and the caudal end of the linear heart tube contributes to the trabeculated portion of the left ventricle (de la Cruz et al., 1989). The present study identified cells in the ventral wall within this inflow region as a subpopulation with a distinct gene expression signature and cell movement; cells at both sides converge to the midline and move upward along the outer curvature. In the chick embryo, the outer curvature is formed by the ventral seam after fusion of the bilateral cardiogenic fields (Abu-Issa and Kirby, 2008). Although in the chick embryo, unlike in the mouse, the bilateral heart fields remain separate until the tube-forming stage without forming the cardiac crescent, the mode of outer curvature formation by midline convergence of bilateral cells might be common to chick and mouse embryos.

The *Ednra-lacZ/EGFP*-expressing cell population is characterized by the presence of cells that express *Tbx5*, which is expressed in a posterior-to-anterior gradient in the inflow region and is important for left ventricular identity (Hoogaars et al., 2007). The *Ednra*-expressing region is distinct from the second heart field, marked by *Isl1* expression. However, *Isl1* expression was detected in both *Ednra-EGFP*-positive and -negative cells at E8.25 in our FACS and RT-PCR experiment. Recently, van den Berg et al. reported that, in chick, an *Isl1*-positive proliferating center caudodorsal to the inflow tract provides cells to the venous and arterial poles of the elongating heart tube (van den Berg et al., 2009). Apparently, *Ednra-lacZ/EGFP*-positive cells are distinct from this population because they are localized to the ventral region of the inflow and are *Isl1*-negative at the crescent/tube-forming stages. However, *Ednra-lacZ/EGFP*-positive cells might also be derived from the *Isl1*-positive pool as *Isl1* is initially expressed in all cardiogenic mesoderm and is downregulated on differentiation (Prall et al., 2007; Yuan and Schoenwolf, 2000). At later stages, many atrial cells express *Ednra-lacZ/EGFP*, suggesting that the second heart field-derived cells may also start to express this gene

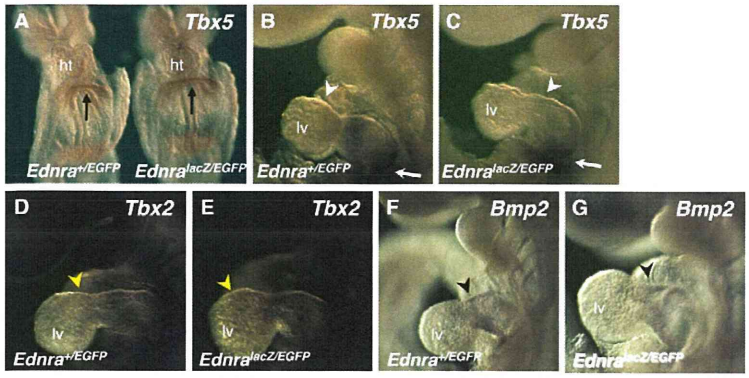

Fig. 9. Changes in *Tbx5* and *Tbx2* expression patterns in *Ednra*-null hearts. (**A**) In situ hybridization of E8.25 $Ednra^{+/EGFP}$ and $Ednra^{lacZ/EGFP}$ hearts. *Tbx5* expression in the inflow region was similar in both hearts (arrows). (**B-G**) In situ hybridization of E9.5 $Ednra^{+/EGFP}$ (B,D,F) and $Ednra^{lacZ/EGFP}$ (C,E,G) hearts for *Tbx5* (B,C), *Tbx2* (D,E) and *Bmp2* (F,G). Anterior expansion of *Tbx5* expression (white arrowheads) was decreased in $Ednra^{lacZ/EGFP}$ hearts, whereas *Tbx5* expression in the posterior (inflow) region (arrows) was similar. By contrast, the *Tbx2*-expressing region (yellow arrowheads) was expanded in $Ednra^{lacZ/EGFP}$ hearts. *Bmp2* expression in the atrioventricular canal (black arrowheads) was similar in $Ednra^{+/EGFP}$ and $Ednra^{lacZ/EGFP}$ hearts. ht, heart tube; lv, left ventricle.

at a later time than do first heart field-derived cells. Thus, *Isl1*-positive cells may eventually express *Ednra*, but the timing might be different between cardiac regions. Indeed, explant culture experiments revealed that *Ednra*-negative cells in the early heart tube might become *Ednra*-positive at later stages, indicating that later *Ednra*-positive cardiomyocytes are derived both from early *Ednra*-positive inflow cells and from tube-forming cells that are *Ednra*-negative at early stages.

According to the ballooning model for chamber formation, which is now widely accepted, the ventricular chambers bulge from the outer curvature of the looped heart (Christoffels et al., 2000). The developing chambers show high proliferative activity and are characterized by the upregulation of chamber-specific myocardial genes. A two-step model has been proposed for this process: the first step is the formation of a primary heart tube and the second step involves localized chamber differentiation in the ventral side (outer curvature) of the heart tube while primary myocardium is continuously recruited at arterial and venous poles of the tube (Christoffels et al., 2000; Moorman and Christoffels, 2003). However, it was not clear when and how chamber-forming cells in the outer curvature are specified. The present study suggests that *Ednra*-positive inflow cells might constitute part of the outer curvature by upward movement and contribute to chamber formation.

Dye-labeling experiments indicated that *Ednra*-positive cells along the outer curvature are derived from the bilateral inflow region. This implies that cells of both sides meet in the midline and distribute mainly to the left lateral wall as a mixed population. Dye labeling also demonstrated a contribution of *Ednra*-positive cells to the right atrial myocardium, although less frequently than to the left atrium. Galli et al. have demonstrated that the left and right sides of the posterior regions of the second heart field contribute to the left and right atrium, respectively (Galli et al., 2008). Thus, the atrial myocardium seems to be derived from at least two different cell sources in a different manner.

Role of endothelin signaling in early heart development

The present study characterizes further the *Ednra*-null phenotype in the early embryonic heart. Ventricular hypoplasia and associated decreased proliferation rates in *Ednra*-null hearts at E9.5 indicate that Ednra-mediated signals are involved in myocardial growth and ventricular formation. Around this stage, Edn1 is secreted by the endothelia of the outflow tract and adjacent vessels (Kurihara et al., 1995) and might act on Ednra-expressing cells arising from the inflow tract in a paracrine manner.

The present result appears to be contradictory to a previous report in which a cardiomyocyte-specific *Ednra*-knockout resulted in no detectable phenotype (Kedzierski et al., 2003). This discrepancy might be explained by the time lag between the start of *Ednra* expression (~E7.8) and myosin heavy chain promoter-driven Cre activation (E8.5-E9.5) (Eckardt et al., 2006; Niu et al., 2005), which might permit *Ednra* expression at early stages. Although it is still possible that the phenotype we describe is an indirect effect of the *Ednra*-null phenotype in other tissues, decreased mitotic frequency in β-galactosidase-positive cells, but not in β-galactosidase-negative cells, of the *Ednra*-null heart supports the possibility that the phenotype is the result of a direct effect on early cardiomyocytes through the Ednra signaling pathway.

The Edn1/Ednra signal is known to induce hypertrophic growth of cardiac myocytes through G_q/G_{11}-mediated activation of the ERK pathway (Sugden, 2003). Consistently, ERK phosphorylation tended to decrease in E9.5 *Ednra*-null hearts and was stimulated by Edn1 treatment. G_q/G_{11}-deficient embryos have severe myocardial hypoplasia in both the compact and trabecular layers, which might account for the mid-gestation lethality of these embryos (Offermanns et al., 1998). These findings lead us to speculate that Edn1/Ednra might be involved in the activation of a G_q/G_{11}-mediated mitotic pathway crucial for early myocardial development.

In addition, *Tbx5* and *Cx40* expression was downregulated in *Ednra*-null hearts and upregulated by stimulation with Edn1. Recent studies have implicated Tbx5 in the regulation of myocardial growth and proliferation (Georges et al., 2008; Goetz et al., 2006) and expression of *Tbx5* is affected by growth factors (Georges et al., 2008). Given these findings, it would be interesting to investigate further the relationship between Edn1/Ednra signaling and Tbx5-dependent myocardial growth/proliferation and chamber specification. Conversely, *Tbx2* expression was expanded towards the left ventricle without changes in *Bmp2* expression in *Ednra*-null hearts. Recently, Aanhaanen et al. reported that *Tbx2*-expressing cells arising in the bilateral limbs of the crescent contribute to the atrioventricular canal and, subsequently, to the *Tbx2*-negative left ventricle, particularly to the basal free wall where *Tbx2* expression is lost (Aanhaanen et al., 2009). In *Tbx2*-null hearts, the atrioventricular canal differentiates prematurely to chamber myocardium and proliferates at increased rates similar to that of chamber myocardium, indicating that Tbx2 might regulate the timing of chamber myocardial differentiation of *Tbx2*-expressing cells allocated to the left ventricular free wall (Aanhaanen et al., 2009). Considering that the *Ednra-lacZ/EGFP*-

positive cell population of the E8.25 heart expresses both *Tbx5* and *Tbx2*, these results raise the possibility that Edn1/Ednra signaling might be involved in chamber formation through the regulation of T-box transcription factor gene expression.

Relationship between cell populations expressing *Ednra* at early and late stages in cardiac development

The present study has revealed that *Ednra-lacZ/EGFP*-expressing cells represent a distinct subset of the first heart field and of the inflow region of the heart, contributing to chamber myocardial formation. Identification of this population has revealed novel aspects of early cell behavior contributing to heart morphogenesis. It has also shown an expansion of *Ednra* expression within chamber-forming cardiomyocytes and implicates the Ednra signal as a mitotic factor and potential regulator of T-box transcription factor gene expression in early cardiac development. The present experiments, investigating cellular distribution/movement and gene expression profiles, indicate that the early *Ednra*-expressing cells contribute partly to the late *Ednra*-expressing population together with cardiomyocytes, which start to express *Ednra* around E9.5 or later. These findings might provide new insight into the understanding of normal cardiac development, which is relevant to the pathogenesis of congenital heart diseases involving abnormalities of chamber morphogenesis.

Acknowledgements

We thank Margaret Buckingham and Margaret Kirby for helpful discussions and comments. We also thank Yuko Fujisawa and Sakura Kushiyama for technical assistance. R.A. is a Research Fellow of the Japan Society for the Promotion of Science (DC1). This work was supported in part by: Global COE Program (Integrative Life Science Based on the Study of Biosignaling Mechanisms), MEXT, Japan; grants-in-aid for scientific research from the Ministry of Education, Culture, Sports, Science and Technology, Japan; grants-in-aid for scientific research from the Ministry of Health, Labour and Welfare of Japan; Mitsubishi Pharma Research Foundation; Japan Cardiovascular Research Foundation; and Mochida Memorial Foundation for Medical and Pharmaceutical Research.

Competing interests statement

The authors declare no competing financial interests.

Supplementary material

Supplementary material for this article is available at
http://dev.biologists.org/lookup/suppl/doi:10.1242/dev.054015/-/DC1

References

Aanhaanen, W. T., Brons, J. F., Dominguez, J. N., Rana, M. S., Norden, J., Airik, R., Wakker, V., de Gier-de Vries, C., Brown, N. A., Kispert, A. et al. (2009). The Tbx2+ primary myocardium of the atrioventricular canal forms the atrioventricular node and the base of the left ventricle. *Circ. Res.* **104**, 1267-1274.

Abu-Issa, R. and Kirby, M. L. (2007). Heart field: from mesoderm to heart tube. *Annu. Rev. Cell Dev. Biol.* **23**, 45-68.

Abu-Issa, R. and Kirby, M. L. (2008). Patterning of the heart field in the chick. *Dev. Biol.* **319**, 223-233.

Araki, K., Araki, M. and Yamamura, K. (2002). Site-directed integration of the cre gene mediated by Cre recombinase using a combination of mutant lox sites. *Nucleic Acids Res.* **30**, e103.

Bruneau, B. G., Logan, M., Davis, N., Levi, T., Tabin, C. J., Seidman, J. G. and Seidman, C. E. (1999). Chamber-specific cardiac expression of Tbx5 and heart defects in Holt-Oram syndrome. *Dev. Biol.* **211**, 100-108.

Bruneau, B. G., Nemer, G., Schmitt, J. P., Charron, F., Robitaille, L., Caron, S., Conner, D. A., Gessler, M., Nemer, M., Seidman, C. E. et al. (2001). A murine model of Holt-Oram syndrome defines roles of the T-box transcription factor Tbx5 in cardiogenesis and disease. *Cell* **106**, 709-721.

Buckingham, M., Meilhac, S. and Zaffran, S. (2005). Building the mammalian heart from two sources of myocardial cells. *Nat. Rev. Genet.* **6**, 826-835.

Cai, C. L., Liang, X., Shi, Y., Chu, P. H., Pfaff, S. L., Chen, J. and Evans, S. (2003). Isl1 identifies a cardiac progenitor population that proliferates prior to differentiation and contributes a majority of cells to the heart. *Dev. Cell* **5**, 877-889.

Cai, C. L., Martin, J. C., Sun, Y., Cui, L., Wang, L., Ouyang, K., Yang, L., Bu, L., Liang, X., Zhang, X. et al. (2008). A myocardial lineage derives from Tbx18 epicardial cells. *Nature* **454**, 104-108.

Chapman, D. L., Garvey, N., Hancock, S., Alexiou, M., Agulnik, S. I., Gibson-Brown, J. J., Cebra-Thomas, J., Bollag, R. J., Silver, L. M. and Papaioannou, V. E. (1996). Expression of the T-box family genes, Tbx1-Tbx5, during early mouse development. *Dev. Dyn.* **206**, 379-390.

Christoffels, V. M., Habets, P. E., Franco, D., Campione, M., de Jong, F., Lamers, W. H., Bao, Z. Z., Palmer, S., Biben, C., Harvey, R. P. et al. (2000). Chamber formation and morphogenesis in the developing mammalian heart. *Dev. Biol.* **223**, 266-278.

Cimini, D., Mattiuzzo, M., Torosantucci, L. and Degrassi, F. (2003). Histone hyperacetylation in mitosis prevents sister chromatid separation and produces chromosome segregation defects. *Mol. Biol. Cell* **14**, 3821-3833.

Clouthier, D. E., Hosoda, K., Richardson, J. A., Williams, S. C., Yanagisawa, H., Kuwaki, T., Kumada, M., Hammer, R. E. and Yanagisawa, M. (1998). Cranial and cardiac neural crest defects in endothelin-A receptor-deficient mice. *Development* **125**, 813-824.

de la Cruz, M. V., Sanchez-Gomez, C. and Palomino, M. A. (1989). The primitive cardiac regions in the straight tube heart (Stage 9⁻) and their anatomical expression in the mature heart: an experimental study in the chick embryo. *J. Anat.* **165**, 121-131.

Delorme, B., Dahl, E., Jarry-Guichard, T., Briand, J. P., Willecke, K., Gros, D. and Theveniau-Ruissy, M. (1997). Expression pattern of connexin gene products at the early developmental stages of the mouse cardiovascular system. *Circ. Res.* **81**, 423-437.

Eckardt, D., Kirchhoff, S., Kim, J. S., Degen, J., Theis, M., Ott, T., Wiesmann, F., Doevendans, P. A., Lamers, W. H., de Bakker, J. M. et al. (2006). Cardiomyocyte-restricted deletion of connexin43 during mouse development. *J. Mol. Cell. Cardiol.* **41**, 963-971.

Galli, D., Dominguez, J. N., Zaffran, S., Munk, A., Brown, N. A. and Buckingham, M. E. (2008). Atrial myocardium derives from the posterior region of the second heart field, which acquires left-right identity as Pitx2c is expressed. *Development* **135**, 1157-1167.

Georges, R., Nemer, G., Morin, M., Lefebvre, C. and Nemer, M. (2008). Distinct expression and function of alternatively spliced Tbx5 isoforms in cell growth and differentiation. *Mol. Cell. Biol.* **28**, 4052-4067.

Goetz, S. C., Brown, D. D. and Conlon, F. L. (2006). TBX5 is required for embryonic cardiac cell cycle progression. *Development* **133**, 2575-2584.

Hoogaars, W. M., Barnett, P., Moorman, A. F. and Christoffels, V. M. (2007). T-box factors determine cardiac design. *Cell. Mol. Life Sci.* **64**, 646-660.

Ishii, Y., Fukuda, K., Saiga, H., Matsushita, S. and Yasugi, S. (1997). Early specification of intestinal epithelium in the chicken embryo: a study on the localization and regulation of CdxA expression. *Dev. Growth Differ.* **39**, 643-653.

Jiang, X., Rowitch, D. H., Soriano, P., McMahon, A. P. and Sucov, H. M. (2000). Fate of the mammalian cardiac neural crest. *Development* **127**, 1607-1616.

Kanegae, Y., Lee, G., Sato, Y., Tanaka, M., Nakai, M., Sakaki, T., Sugano, S. and Saito, I. (1995). Efficient gene activation in mammalian cells by using recombinant adenovirus expressing site-specific Cre recombinase. *Nucleic Acids Res.* **23**, 3816-3821.

Kedzierski, R. M., Grayburn, P. A., Kisanuki, Y. Y., Williams, C. S., Hammer, R. E., Richardson, J. A., Schneider, M. D. and Yanagisawa, M. (2003). Cardiomyocyte-specific endothelin A receptor knockout mice have normal cardiac function and an unaltered hypertrophic response to angiotensin II and isoproterenol. *Mol. Cell. Biol.* **23**, 8226-8232.

Kelly, R. G., Brown, N. A. and Buckingham, M. E. (2001). The arterial pole of the mouse heart forms from Fgf10-expressing cells in pharyngeal mesoderm. *Dev. Cell* **1**, 435-440.

Kirby, M. (2007). *Cardiac Development*. New York: Oxford University Press.

Koibuchi, N. and Chin, M. T. (2007). CHF1/Hey2 plays a pivotal role in left ventricular maturation through suppression of ectopic atrial gene expression. *Circ. Res.* **100**, 850-855.

Kokubo, H., Tomita-Miyagawa, S., Hamada, Y. and Saga, Y. (2007). Hesr1 and Hesr2 regulate atrioventricular boundary formation in the developing heart through the repression of Tbx2. *Development* **134**, 747-755.

Kurihara, Y., Kurihara, H., Suzuki, H., Kodama, T., Maemura, K., Nagai, R., Oda, H., Kuwaki, T., Cao, W. H., Kamada, N. et al. (1994). Elevated blood pressure and craniofacial abnormalities in mice deficient in endothelin-1. *Nature* **368**, 703-710.

Kurihara, Y., Kurihara, H., Oda, H., Maemura, K., Nagai, R., Ishikawa, T. and Yazaki, Y. (1995). Aortic arch malformations and ventricular septal defect in mice deficient in endothelin-1. *J. Clin. Invest.* **96**, 293-300.

Laugwitz, K. L., Moretti, A., Caron, L., Nakano, A. and Chien, K. R. (2008). Islet1 cardiovascular progenitors: a single source for heart lineages? *Development* **135**, 193-205.

Maemura, K., Kurihara, H., Kurihara, Y., Oda, H., Ishikawa, T., Copeland, N. G., Gilbert, D. J., Jenkins, N. A. and Yazaki, Y. (1996). Sequence analysis, chromosomal location, and developmental expression of the mouse preproendothelin-1 gene. *Genomics* **31**, 177-184.

Meilhac, S. M., Esner, M., Kelly, R. G., Nicolas, J. F. and Buckingham, M. E. (2004). The clonal origin of myocardial cells in different regions of the embryonic mouse heart. *Dev. Cell* **6**, 685-698.
Mjaatvedt, C. H., Nakaoka, T., Moreno-Rodriguez, R., Norris, R. A., Kern, M. J., Eisenberg, C. A., Turner, D. and Markwald, R. R. (2001). The outflow tract of the heart is recruited from a novel heart-forming field. *Dev. Biol.* **238**, 97-109.
Moorman, A. F. and Christoffels, V. M. (2003). Cardiac chamber formation: development, genes, and evolution. *Physiol. Rev.* **83**, 1223-1267.
Nagy, A., Gertsenstein, M., Vintersten, K. and Behringer, R. (2003). *Manipulating the Mouse Embryo: a Laboratory Manual*, 3rd edn. Cold Spring Harbor, NY: Cold Spring Harbor Laboratory Press.
Niu, Z., Yu, W., Zhang, S. X., Barron, M., Belaguli, N. S., Schneider, M. D., Parmacek, M., Nordheim, A. and Schwartz, R. J. (2005). Conditional mutagenesis of the murine serum response factor gene blocks cardiogenesis and the transcription of downstream gene targets. *J. Biol. Chem.* **280**, 32531-32538.
Offermanns, S., Zhao, L. P., Gohla, A., Sarosi, I., Simon, M. I. and Wilkie, T. M. (1998). Embryonic cardiomyocyte hypoplasia and craniofacial defects in G alpha q/G alpha 11-mutant mice. *EMBO J.* **17**, 4304-4312.
Ozeki, H., Kurihara, Y., Tonami, K., Watatani, S. and Kurihara, H. (2004). Endothelin-1 regulates the dorsoventral branchial arch patterning in mice. *Mech. Dev.* **121**, 387-395.
Prall, O. W., Menon, M. K., Solloway, M. J., Watanabe, Y., Zaffran, S., Bajolle, F., Biben, C., McBride, J. J., Robertson, B. R., Chaulet, H. et al. (2007). An Nkx2-5/Bmp2/Smad1 negative feedback loop controls heart progenitor specification and proliferation. *Cell* **128**, 947-959.
Sato, T., Kawamura, Y., Asai, R., Amano, T., Uchijima, Y., Dettlaff-Swiercz, D. A., Offermanns, S., Kurihara, Y. and Kurihara, H. (2008a). Recombinase-mediated cassette exchange reveals the selective use of Gq/G11-dependent and -independent endothelin 1/endothelin type A receptor signaling in pharyngeal arch development. *Development* **135**, 755-765.
Sato, T., Kurihara, Y., Asai, R., Kawamura, Y., Tonami, K., Uchijima, Y., Heude, E., Ekker, M., Levi, G. and Kurihara, H. (2008b). An endothelin-1 switch specifies maxillomandibular identity. *Proc. Natl. Acad. Sci. USA* **105**, 18806-18811.
Schaart, G., Viebahn, C., Langmann, W. and Ramaekers, F. (1989). Desmin and titin expression in early postimplantation mouse embryos. *Development* **107**, 585-596.
Srivastava, D., Cserjesi, P. and Olson, E. N. (1995). A subclass of bHLH proteins required for cardiac morphogenesis. *Science* **270**, 1995-1999.
Sugden, P. H. (2003). An overview of endothelin signaling in the cardiac myocyte. *J. Mol. Cell. Cardiol.* **35**, 871-886.
Takeuchi, J. K., Ohgi, M., Koshiba-Takeuchi, K., Shiratori, H., Sakaki, I., Ogura, K., Saijoh, Y. and Ogura, T. (2003). Tbx5 specifies the left/right ventricles and ventricular septum position during cardiogenesis. *Development* **130**, 5953-5964.
van den Berg, G., Abu-Issa, R., de Boer, B. A., Hutson, M. R., de Boer, P. A., Soufan, A. T., Ruijter, J. M., Kirby, M. L., van den Hoff, M. J. and Moorman, A. F. (2009). A caudal proliferating growth center contributes to both poles of the forming heart tube. *Circ. Res.* **104**, 179-188.
Waldo, K. L., Kumiski, D. H., Wallis, K. T., Stadt, H. A., Hutson, M. R., Platt, D. H. and Kirby, M. L. (2001). Conotruncal myocardium arises from a secondary heart field. *Development* **128**, 3179-3188.
Wilkinson, D. (1992). *In Situ Hybridization: a Practical Approach.* Oxford, UK: IRL Press.
Yamada, M., Revelli, J. P., Eichele, G., Barron, M. and Schwartz, R. J. (2000). Expression of chick Tbx-2, Tbx-3, and Tbx-5 genes during early heart development: evidence for BMP2 induction of Tbx2. *Dev. Biol.* **228**, 95-105.
Yanagisawa, H., Hammer, R. E., Richardson, J. A., Williams, S. C., Clouthier, D. E. and Yanagisawa, M. (1998). Role of Endothelin-1/Endothelin-A receptor-mediated signaling pathway in the aortic arch patterning in mice. *J. Clin. Invest.* **102**, 22-33.
Yuan, S. and Schoenwolf, G. C. (2000). Islet-1 marks the early heart rudiments and is asymmetrically expressed during early rotation of the foregut in the chick embryo. *Anat. Rec.* **260**, 204-207.
Zhou, B., Ma, Q., Rajagopal, S., Wu, S. M., Domian, I., Rivera-Feliciano, J., Jiang, D., von Gise, A., Ikeda, S., Chien, K. R. et al. (2008). Epicardial progenitors contribute to the cardiomyocyte lineage in the developing heart. *Nature* **454**, 109-113.

Endothelin receptor type A expression defines a distinct cardiac subdomain within the heart field and is later implicated in chamber myocardium formation

DEV054015 Supplementary Material

Files in this Data Supplement:

- **Supplemental Figure S1** -

Fig. S1. Recombinase-mediated knock-in of *EGFP* into the *Ednra* allele.

- **Supplemental Figure S2** -

Fig. S2. *Ednra-lacZ*/*EGFP* and endogenous gene expression patterns. (**A-D**) Whole-mount (A,B) and section (C,D) staining for β-galactosidase activity (A,C) and *Ednra* in situ hybridization (B,D) in E8.5 hearts. Arrows indicate signals from the inflow region towards the left ventricle along the outer curvature. ift, inflow tract. (**E**) Comparison of *Ednra-EGFP* with *Tbx5* expression in E8.25 hearts. Planes of section (a, b and c) are indicated in the diagram on the right. Sections were subjected to immunostaining for EGFP or in situ hybridization for *Tbx5*. Boxed areas in a are magnified in a'. *Ednra-EGFP* and *Tbx5* are co-expressed in the ventral wall of the inflow region (arrowheads).

- **Supplemental Figure S3** -

Fig. S3. Explant culture of E8.25 *Ednra*$^{+/EGFP}$ heart tube regions. (**A-H**) Phase-contrast (A,B,E,F) and fluorescent (C,D,G,H) images of explants from the ventricular (A-D) and inflow (E-F) regions. At the start of culture, EGFP signals were clearly detectable in the inflow region (arrow in G), whereas the signals in the ventricular region were very low (C). After 24 hours, both ventricular and inflow regions demonstrated intense EGFP signals (D,H).

- **Supplemental Figure S4** -

Fig. S4. Whole-mount β-galactosidase staining on *Ednra*$^{lacZ/+}$ and *Ednra*$^{lacZ/EGFP}$ hearts at E9.5. (**A,B**) Caudal (posterior) views of E9.5 *Ednra*$^{lacZ/+}$ (A) and *Ednra*$^{lacZ/EGFP}$ (B) hearts stained for β-galactosidase activity. *Ednra*$^{lacZ/EGFP}$ hearts show a lower distribution of *lacZ*-positive cells to the posterior wall of the right ventricle than do *Ednra*$^{lacZ/+}$ hearts. lv, left ventricle; rv, right ventricle. White arrowheads indicate boundaries of *lacZ* expression.

- **Supplemental Table S1** -

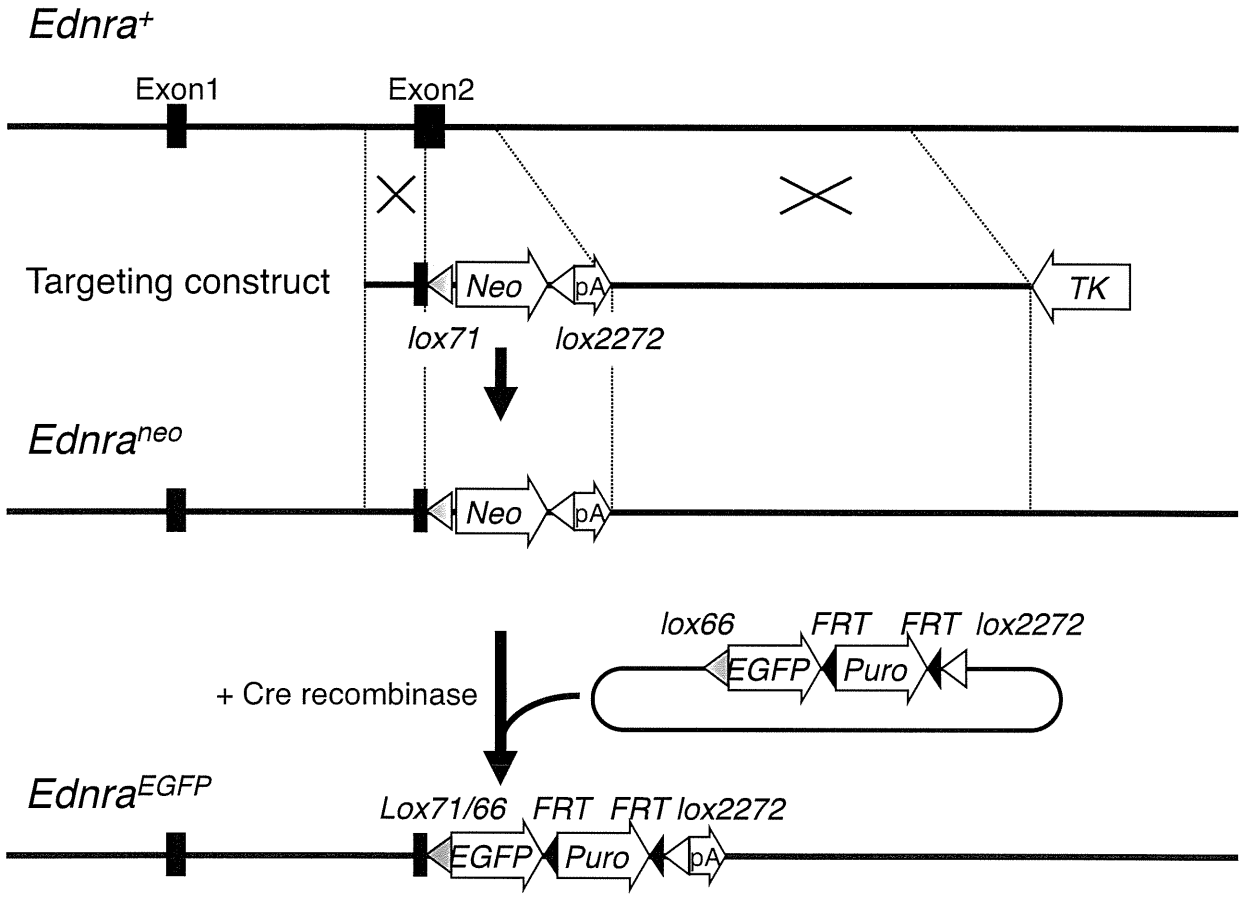
Ednra+
Exon1
Exon2
Targeting construct
Neo
pA
TK
lox71
lox2272
Ednraneo
Neo
pA
lox66
FRT
FRT
lox2272
+ Cre recombinase
EGFP
Puro
EdnraEGFP
Lox71/66
FRT
FRT
lox2272
EGFP
Puro
pA

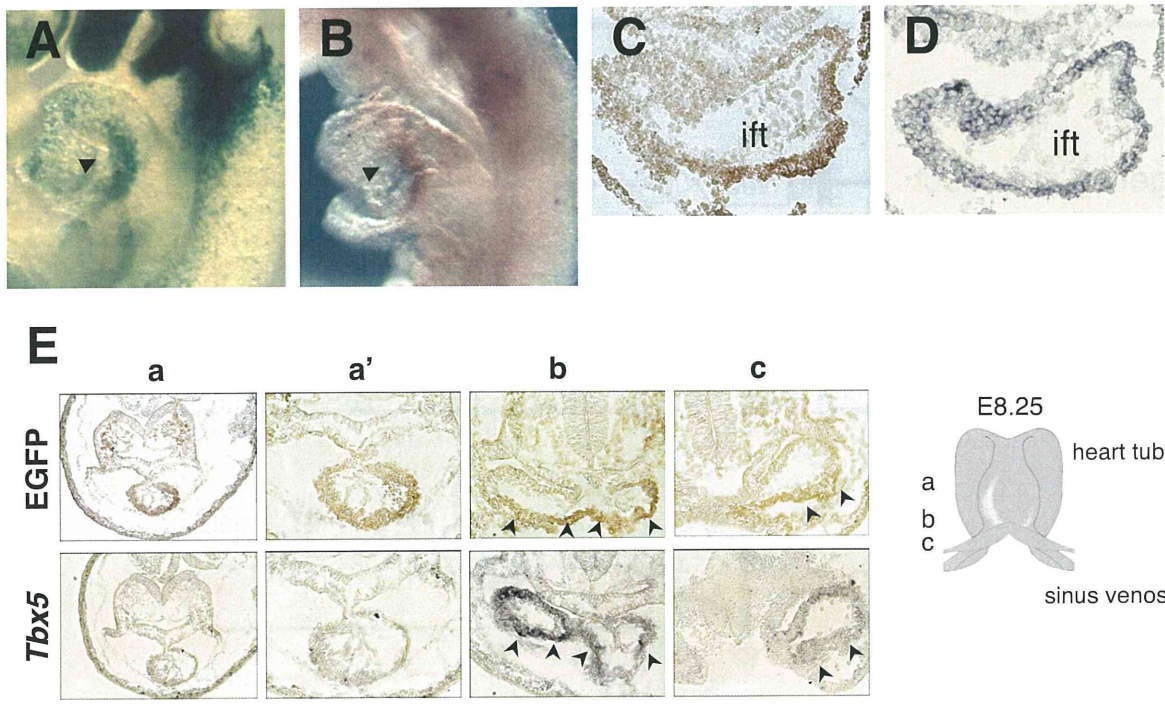
A
B
C
ift
D
ift
E
a
a'
b
c
EGFP
Tbx5
E8.25
heart tube
a
b
c
sinus venosus

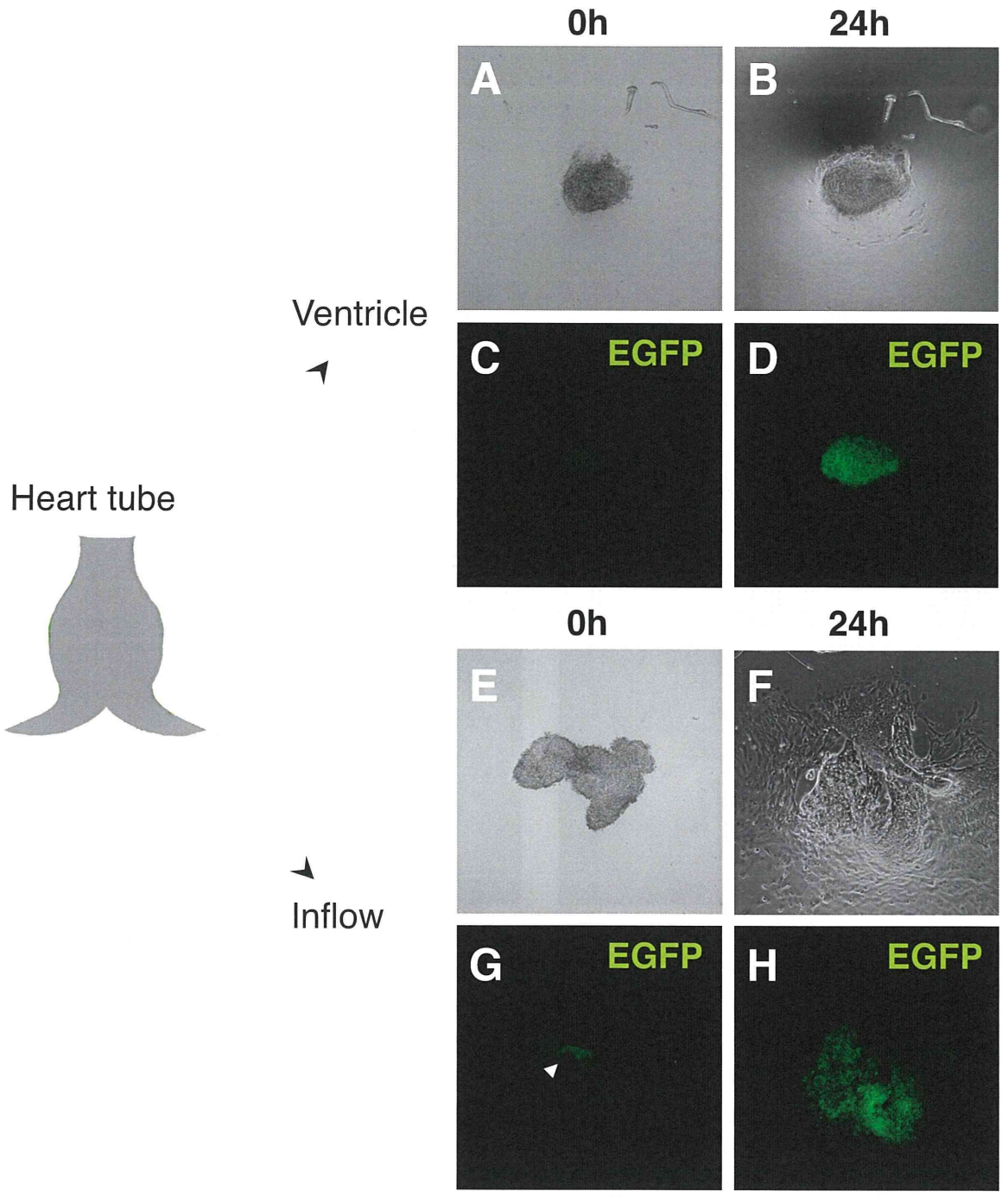
0h
24h
A
B
Ventricle
C
EGFP
D
EGFP
Heart tube
0h
24h
E
F
Inflow
G
EGFP
H
EGFP

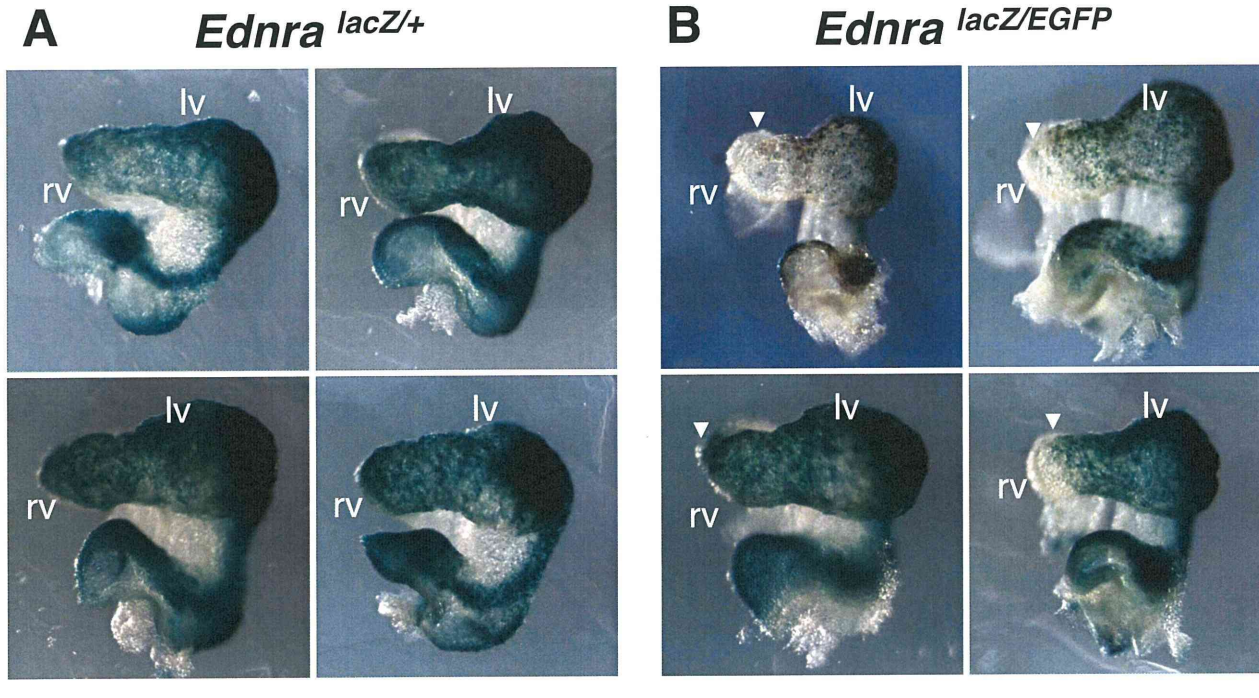
A
Ednra lacZ/+
lv
rv
lv
rv
lv
rv
lv
rv
B
Ednra lacZ/EGFP
lv
rv
lv
rv
lv
rv
lv
rv

Table S1. Primers and reaction conditions for RT-PCR analysis

Gene	Accession number	Forward (5′-3′)	Reverse (5′-3′)	Amplicon length (bp)	Annealing temperature (°C)
Conventional RT-PCR					
Cx40	NM_008121	TGGGCAGTTGAACAGCAGCCAG	CCCAGGAAGCTCCAGTCACCCA	119	60
Ednra	NM_010332.2	ACGCTGGCCTTTCG	CTGAGCAGTTCACACCGGTTCTTATC	603	61
EGFP	U57609.1	GACGTAAACGGCCACAAGTTCA	GAACTCCAGCAGGACCATGTGATC	608	61
Gapdh	XR_030830.1	GGTGTGAACCACGAGAAATAT	AGATCCACGACGGACACATT	334	61
Hand1	NM_008213.2	GGAGTTGCCTCAGCAGCCCG	CCGTAGCCGCTGCGTCCTTT	200	60
Isl1	NM_021459.3	GCCTGCAGCCGACAGCTCAT	AGGTCCGCAAGGTGTGCAGC	271	60
Nkx2.5	NM_008700.2	CCCAGCCGCCCCCACATTTT	GCGCCATCCGTCTCGGCTTT	132	60
Tbx2	NM_009324.2	CGAGATGCCTAAACGCATG	CAAGATGTCATTGGCTCGCAC	190	60
Tbx5	NM_011537.2	ACACATGGCCCAGCATGCCC	CCCGCACTGCCTGACCACAG	138	60
Tbx18	NM_023814.3	GGTATGTTTACCATAGCTCT	AAGGTGAGAGTCCGTAGTGAT	472	60
Real time PCR					
Hand1	NM_008213.2	GGAGTTGCCTCAGCAGCCCG	CCGTAGCCGCTGCGTCCTTT	200	61
HPRT	NM_013556.2	AGCGCAAGTTGAATCTGC	AGCGACAATCTACCAGAG	119	60
Nkx2.5	NM_008700.2	CCCAGCCGCCCCCACATTTT	GCGCCATCCGTCTCGGCTTT	132	61
Tbx5	NM_011537.2	ACACATGGCCCAGCATGCCC	CCCGCACTGCCTGACCACAG	138	61

RESEARCH ARTICLE

Establishment of Mice Expressing EGFP in the Placode-Derived Inner Ear Sensory Cell Lineage and FACS-Array Analysis Focused on the Regional Specificity of the Otocyst

Chisato Fujimoto,[1,2] Hidenori Ozeki,[1,2] Yasunobu Uchijima,[1] Keigo Suzukawa,[2] Akihisa Mitani,[1,3] Shigetomo Fukuhara,[4] Koichi Nishiyama,[1] Yukiko Kurihara,[1] Kenji Kondo,[2] Hiroyuki Aburatani,[5] Kimitaka Kaga,[2] Tatsuya Yamasoba,[2] and Hiroki Kurihara[1]*

[1]Department of Physiological Chemistry and Metabolism, Graduate School of Medicine, The University of Tokyo, Bunkyo-ku, Tokyo, 113-0033, Japan
[2]Department of Otolaryngology, Graduate School of Medicine, The University of Tokyo, Bunkyo-ku, Tokyo, 113-8655, Japan
[3]Department of Respiratory Medicine, Graduate School of Medicine, The University of Tokyo, Bunkyo-ku, Tokyo, 113-8655, Japan
[4]Department of Structural Analysis, National Cardiovascular Center Research Institute, Suita, Osaka, 565-8565, Japan
[5]Genome Science Division, Research Center for Advanced Science and Technology, The University of Tokyo, Meguro-ku, Tokyo, 153-8904, Japan

ABSTRACT

In this study, we established a novel enhanced green fluorescent protein (EGFP) reporter mouse line that enables the visualization of the placode-derived inner ear sensory cell lineage. EGFP was initially expressed in the otic placode and throughout its differentiation process into the inner ear sensory patches. At embryonic day 10.5 (E10.5), EGFP was expressed in the ventral and dorsomedial region of the otocyst. These regions could mainly give rise to the cochlea, including the organ of Corti, and the saccule, including the macula and the endolymphatic duct. The region could also give rise to cells that will develop as either prosensory cells or statoacoustic ganglion neuroblasts. By using this line and fluorescence-activated cell sorting (FACS)-array technology, we developed a new gene expression profile of the regional specificity of the otocyst. EGFP-positive regions include the *Otx1*-positive region, which could be clearly distinguished from EGFP-negative regions. The signal log ratio of microarray data showed high efficiency in predicting the genes expressed mainly in the ventral and/or dorsomedial otocyst and the data could be mined to uncover many novel genes involved in inner ear morphogenesis and cell fate regulation. Additionally, these data suggest that some novel genes enriched in EGFP-positive regions may be potentially involved in human congenital sensorineural hearing loss. This reporter line could play important roles in the use of animal models for detailed analysis of the differentiation process into the sensory patches and the identification of regional-specific gene networks and novel gene functions in the developing inner ear. J. Comp. Neurol. 518:4702–4722, 2010.

INDEXING TERMS: transgenic mice; green fluorescent protein; inner ear; fluorescence-activated cell sorting; gene expression profiling; receiver operating characteristic

The inner ear of vertebrates is a complex sensory structure that derives from ectodermal thickenings of the head called otic placodes (Kaufman and Bard, 1999; Kiernan et al., 2002). The acquisition of inner ear axial identity from surrounding tissues probably begins after otic placode formation and involves early cell fate decisions (Bok et al., 2007). These early cell fate decisions can be classified into neural-fated cells, prosensory cells, and nonsensory epithelial cells. Neural-fated cells delaminate from the otic epithelium to form neurons of the statoacoustic

Additional Supporting Information may be found in the online version of this article.

Grant sponsor: the Global COE Program (Integrative Life Science Based on the Study of Biosignaling Mechanisms) (MEXT), the Ministry of Education, Culture, Sports, Science, and Technology Japan; Grant number: 21390238; Grant sponsor: the Ministry of Health, Labor, and Welfare of Japan; Grant number: H21-Seibutsushigen-Ippan-001.

*CORRESPONDENCE TO: Hiroki Kurihara, Department of Physiological Chemistry and Metabolism, Graduate School of Medicine, The University of Tokyo, 7-3-1, Hongo, Bunkyo-ku, Tokyo 113-0033, Japan.
E-mail: kuri-tky@umin.ac.jp

Received February 11, 2010; Revised June 2, 2010; Accepted July 1, 2010
DOI 10.1002/cne.22468
Published online July 26, 2010 in Wiley Online Library (wileyonlinelibrary.com)

ganglion (SAG) (Carney and Silver, 1983; Rubel and Fritzsch, 2002). Prosensory cells differentiate into mechanosensory hair cells and nonsensory supporting cells (Kelley et al., 1995; Fekete et al., 1998). The sense of hearing and equilibrium in vertebrates are controlled by epithelial sensory patches in the cochlea and vestibule of the inner ear and their dominant neurons. Many genes induced within the otic epithelium as a result of axial specificity continue to mediate inner ear morphogenesis, such as the interaction between prosensory and nonsensory epithelial cells (Bok et al., 2007). Elucidating the signals providing axial specificity, the resultant molecular events from existing signals, and the regional-specific genes related to neural/sensory organ formation is important in understanding inner ear morphogenesis.

One major approach to clarify the novel molecular mechanism of the morphogenesis is to reliably profile the spatiotemporal expression of genes within this complex organ. Several microarray expression profiling studies of the murine inner ear have been reported (Chen and Corey, 2002; Liu et al., 2004; Powles et al., 2004; Morris et al., 2005; Sajan et al., 2007). Although these studies may contribute to identifying and analyzing expressed genes, more powerful tools for dissecting genetically, morphologically, and/or regionally defined cell populations for transcriptome analysis are required. The combination of the green fluorescent protein (GFP) reporter strain and the fluorescence-activated cell sorting (FACS) system has allowed sampling of purified cell populations (Lobo et al., 2006; Marsh et al., 2008). To date, none of these approaches have been attempted during the developmental stage of the inner ear.

GFP reporter mice have been widely used for the imaging of biologically important cell populations. For analysis of the developing inner ear, previous studies have used some reporter lines in which GFP expression is driven by promoters of the sine oculis related homeobox 1 homolog (*Drosophila*) (*Six1*) (Ozaki et al., 2004) and the mouse homolog of the *Drosophila* atonal gene (*Math1*) (Lumpkin et al., 2003). For example, *Six1*-expressing cells were detected by GFP luminescence in heterozygous embryos from the otic placode to the nonsensory area of the cochlea (Ozaki et al., 2004). After division into vestibular and auditory compartments, the *Math1*-GFP reporter system can be a powerful tool to monitor the differentiation of the prosensory precursors to hair cells (Lumpkin et al., 2003). However, to our knowledge, there are no lines for spatiotemporally monitoring the cell lineage from the otic placode to both sensory and neural cell differentiation.

In the present study, we established transgenic mouse lines in which enhanced GFP (EGFP) expression was driven by the promoter of endothelin receptor type A gene (*Ednra*). One of the lines exhibited ectopic EGFP expression in the developing inner ear. EGFP expression was initially detected in the otic placode and throughout its differentiation into the inner ear sensory patches. This line has unprecedented significance as a reporter system to monitor the placode-derived sensory cell lineage during inner ear development. We focused on the E10.5 stage, when EGFP expression of the transgenic line was detected mainly in the ventral and dorsomedial regions of the otocyst. The otocyst undergoes a sequence of further evaginations and tissue remodelings to form the embryonic inner ear, which is divided into vestibular and auditory compartments. At this stage, transcription could be active in the already existing signals related to axial specificity and in regionally specific genes including genes related to neural/sensory organ formation. We sorted the otocyst epithelial cells into EGFP-positive and EGFP-negative cells, profiled the expression of the genes in FACS-enriched cell population, and conducted transcriptome analysis. The use of this novel transgenic line and FACS-array technology in the present study provides an insight into a comprehensive understanding of the molecular mechanisms underlying organogenesis and cell fate regulation in the inner ear.

MATERIALS AND METHODS

Construction of Ednra-EGFP transgenic mice

The *Ednra-EGFP* transgene used for generation of transgenic mice was constructed as follows. The *EGFP* coding sequence flanked by *Eco*RI and *Xho*I restriction sites (~0.7 kb) was generated from the pIRES2-EGFP vector (Clontech, Palo Alto, CA) by polymerase chain reaction (PCR) with 5′-GAATTCAACCATGGTGAGCAAG-3′ (forward primer) and 5′-CTCGAGTTACTTGTACAGCTCG-3′ (reverse primer). The EGFP coding sequence was subsequently ligated into the pCEFL-HA vector (Murga et al., 1998) via the *Eco*RI-*Xho*I restriction site to yield the *EGFP*-pCEFL-HA vector. A polyadenylation signal from bovine growth hormone (BGHpA) was located downstream of the EGFP coding sequence in the *EGFP*-pCEFL-HA vector.

The *Ednra* sequence, containing the promoter region and exon1 of the mouse *Ednra* gene, flanked by *Eco*RI restriction sites, was generated by genomic PCR with 5′-GAATTCTTTCTCTCTGAATATTTAAC-3′ (forward primer) and 5′-CTTAAGAGCTCCTCGGAAGCAGACA-3′ (reverse primer). The *Ednra* sequence was ligated into the *EGFP*-pCEFL-HA vector to construct a ~ 3.2-kb *Ednra-EGFP*-BGHpA sequence. A *Ednra-EGFP*-BGHpA fragment obtained by restriction digestion with the *Eco*RI and *Pvu*II enzymes was excised from the pCEFL-HA vector, purified, and injected into fertilized eggs with C57BL/6 genetic backgrounds. Founder animals were identified by Southern blot analysis by using an *EGFP*-specific ^{32}P-labeled

probe, and progenies were routinely detected by PCR with transgene-specific oligonucleotides (data not shown). We have established several *Ednra-EGFP* transgenic mouse lines with the *Ednra-EGFP* transgene. One line, named *Tg(ETAR-EGFP)14Imeg* (hereafter termed Line-14), exhibited ectopic EGFP expression in the developing inner ear. Another line, named *Tg(ETAR-EGFP)1Imeg* (hereafter termed Line-1), exhibited no ectopic expression in the ear and served as the control in genomic analysis.

All procedures were carried out in accordance with the University of Tokyo Animal Care Protocols and the National Institutes of Health *Guide for the Care and Use of Laboratory Animals*.

Southern blot analysis

Genomic DNA was extracted from a part of the tails of the mice by the standard technique and digested with an appropriate restriction enzyme, electrophoresed in a 0.8% agarose gel, transferred to a Nytran SuPerCharge membrane (Schleicher & Schuell Bioscience, Keene, NH), and hybridized with the EGFP portion of the transgene radiolabeled with [^{32}P]deoxycytidine triphosphate. Then 657 bp of the EGFP sequence, which was used as the template to synthesize the radiolabeled probe, was generated by PCR with 5′-AGCTGGACGGCGACGTAAAC-3′ (forward primer) and 5″-CTCGTCCATGCCGAGAGTGA-3′ (reverse primer). The probe was constructed by using Megaprime DNA labeling systems (Amersham Biosciences, Piscataway, NJ). Membranes were washed under high stringency conditions and autoradiographs were obtained.

Colony PCR-based screening

Line-14 genomic DNA fragments digested with *Eco*RI were electrophoresed in an agarose gel, and ~2.8-kb fragments were dissected from the gel and purified by using Wizard SV Gel and PCR Clean-Up System (Promega, Madison, WI) following the manufacturer's instructions. The fragments were ligated into the vector pCRII-TOPO (Invitrogen, Carlsbad, CA) according to the manufacturer's instructions. The resulting construct was transformed to DH5-alpha by 37°C heat shock. The transformation solution in SOC medium was plated on an appropriate LB-agar/ampicillin (100 μg/ml) plate and incubated overnight at 37°C. Colonies picked from the plate were used as templates for PCR amplification. The above-mentioned EGFP-specific primers were used for colony PCR. We selected clones that possessed the EGFP sequence, and the construct was then sequenced.

Genome walking method

To identify the integrated regions of the transgene, libraries were constructed by using the GenomeWalker Universal Kit (Clontech, Mountain View, CA). Homozygous Line-14 and wild-type genomic DNA were digested separately with four restriction enzymes—*Eco*RV, *Dra*I, *Pvu*II, and *Stu*I. Digested DNA was purified according to the manufacturer's protocol. A GenomeWalker adaptor was ligated to both ends of the digested, purified DNA. Gene-specific primers were designed within the promoter region of the *Ednra* gene (gsp1 5′-GGATTGTCAGGG GTGCTGAGAGGCAAA-3′; gsp2 5′-ACTCCTGACTACTGAG GCAACAGCAGT-3″, and the BGHpA region (gsp1 5′-GAG GATTGGGAAGACAATAGCAGGCA-3′; gsp2 5′-GGATGCG GTGGGCTCTATGGCTTCTGA-3a′). The primary PCR reaction was carried out with the AP1 adaptor and gsp1 primers; subsequent nested PCR was carried out with the AP2 adaptor and gsp2 primers. The PCR cycling conditions were established according to the manufacturer's protocol. Amplification was performed on a GeneAmp PCR System 9700 (Applied Biosystems, Foster City, CA). Products were visualized on a 1.5% agarose gel and gel-purified by using Wizard SV Gel and PCR Clean-Up System (Promega) according to the manufacturer's instructions. Products were directly sequenced without cloning.

Auditory and vestibular function tests

The vestibular function of mice was assessed with the swim test (Khan et al., 2004). Normal mice could swim with their heads above water for the entire 60 seconds; however, mice with vestibular dysfunction could keep their heads above water for no more than a few seconds (Khan et al., 2004). Here, 2-month-old mice were placed in a cage filled with water at room temperature for 60 seconds. The average swimming time with the head above water was determined for three trials for each mouse.

The auditory function of mice was evaluated by their auditory brainstem response (ABR) at 2 months of age. ABR is an evoked potential measurement of auditory activity of the cochlea, auditory nerve, and central auditory pathway in the brainstem. It is often used as a technique in auditory research in humans and laboratory animals (Pourbakht and Yamasoba, 2003). Homozygous and heterozygous 2-month-old *Ednra-EGFP* Line-14 transgenic mice and wild-type controls were anesthetized with a mixture of xylazine hydrochloride (10 mg/kg, i.m.) and ketamine hydrochloride (40 mg/kg, i.m.). Before the ABR test, the tympanic membranes or tympanic cavities were confirmed to be normal in all mice. When the paw pinch reflex disappeared, three electrodes were placed subcutaneously on the vertex of the head (active electrode), in the

TABLE 1.
Primary Antibodies Used in Immunohistochemistry

Antigen	Immunogen	Manufacturer	Dilution
Green Flourescent Protein (GFP)	Full length amino acid sequence derived from *Aequorea victoria*.	Abacam (Cambridge, MA, USA), goat polyclonal, ab6673	1:100
Myosin 7a (Myo7a)	Amino acids 880-1077 from the tail region of human myosin 7a.	Proteus Biosciences (Ramona, CA, USA), rabbit polyclonal, 25-6790	1:100
$P^{27^{kip1}}$	Amino acids 175-198 derived from c-terminal of human $P^{27^{kip1}}$.	Thermo Fisher Scientific (Fremont, CA, USA), rabbit polyclonal, RB-9019	1:100
SRY-box containing gene 2 (Sox2)	Synthetic peptide (sequence, SSSPPVVTSSSHSRAPC) from human Sox2. The immunogen sequence iis dentical in human and mouse.	Chemicon (Temecula, CA, USA), rabbit polyclonal, AB5603	1:1000

postauricular region of the measured ear (reference electrode), and in the postauricular region of the opposite ear (ground). The speaker was located 10 cm from the tragus of the stimulated ear. A tone burst stimulus (2, 4, 8, 16, and 32 kHz) was produced by using a sound stimulator (Neuropack Σ MEB-5504; Nihon Kohden, Tokyo, Japan). The duration of the stimulus was 15 milliseconds, the presentation rate was 11/second, and the rise/fall time was 1 millisecond. At each intensity level (5-dB steps) to assess the threshold, the ABR was determined by averaging 500 responses. The threshold was visually defined as the lowest intensity level at which a clear reproducible waveform was visible in the trace. An overall test for differences among homozygous Line-14 mice, heterozygous Line-14 mice, and wild-type controls was performed for each frequency by using one-way analysis of variance (ANOVA) ($P < 0.05$). Statistical analyses were conducted by using SPSS version 11.0J (SPSS Japan, Tokyo, Japan).

Antibody characterization

All antibodies used in this study are listed in Table 1. The GFP antibody recognized the expected (27-kDa) band on a Western blot of GFP-positive transgenic rat aorta and showed no cross-reactivity with the rat endogenous arterial proteins mentioned in a previous report (Rodriguez-Menocal et al., 2009). In the present study, the antibody stained the inner ear in Line-14 EGFP-positive transgenic mice but not in wild-type mice (Fig. 1). The myosin 7a (*Myo7a*) antibody displayed the classic hair cell-specific labeling distribution (Hasson et al., 1995; Bermingham-McDonogh et al., 2006) and exhibited similar labeling in a variety of species including the mouse (Hasson et al., 1997). The $p27^{kip1}$ antibody recognized the expected (27-kDa) band on a Western blot of murine neonatal organ of Corti (Chen and Segil, 1999). $p27^{kip1}$ immunohistochemistry showed staining in the primordial organ of Corti and differentiated supporting cells of the mature organ of Corti (Chen and Segil, 1999). The appropriate controls of the SRY- box containing gene 2 (*Sox2*) antibody for Western blotting are mouse or human embryonic stem cell lysate and mouse embryonic germ cell lysate (manufacturer's datasheet). The antibody recognized a 34-kDa band corresponding to *Sox2* on Western blots of whole cell or nuclear extracts; this band was not observed in cytosolic extracts. The antibody stained tissue in wild-type mice but not in conditional *Sox2*-knockout mice (Favaro et al., 2009).

Histological and immunohistochemical analyses

The tissues of adult mice were fixed by cardiac perfusion with ice-cold 4% paraformaldehyde (PFA) in phosphate-buffered saline (PBS; pH 7.4) followed by decapitation. Mouse embryos were fixed in 4% PFA in PBS. For adults, the heads were fixed in 4% PFA in PBS and decalcified in 10% ethylenediamine tetraacetic acid for several days. Then the specimens were dehydrated in ethanol series and embedded in paraffin. The paraffin block containing the tissue was cut into 4-μm sections. The sections were deparaffinized and then rehydrated through xylene and ethanol series. For hematoxylin-eosin staining, the sections were stained with Carrazi's hematoxylin (Muto Pure Chemicals, Tokyo, Japan), treated with 1% HCl in 70% ethanol for differentiation, stained in eosin solution (1% Eosin Y [Merck, Darmstadt, Germany]:80% ethanol/glacial acetic acid = 100:375:1 [v/v/v]), dehydrated, and mounted.

For immunohistochemical staining, the sections were placed in citrate-buffered solution (pH 6.0; Dako Cytomation Japan, Kyoto, Japan) and autoclaved at 121°C for 20 minutes for antigen retrieval. Sections were incubated for 1 hour with a blocking solution (PBS [pH 7.4] containing 5% skim milk [Wako, Osaka, Japan], 0.1% Triton-X 100, and 0.1% sodium azide) at room temperature to reduce nonspecific antibody binding. The sections were then incubated with primary antibody overnight at 4°C in the blocking solution.. The secondary antibodies used were Alexa Fluor 488 donkey anti-goat IgG (Invitrogen; 1:200

in blocking solution), Alexa Fluor 555 donkey anti-rabbit IgG (Invitrogen; 1:200 in blocking solution), and Alexa Fluor 594 goat anti-rabbit IgG (Invitrogen; 1:200 in blocking solution). The sections were mounted with ProLong Gold Antifade Reagent (Invitrogen). The final images were corrected for brightness and contrast, and color-converted from red-green to magenta-green by using Adobe Photoshop 7.0 (Adobe Systems, San Jose, CA).

β-Galactosidase staining

Mouse embryos were fixed in 4% PFA in PBS. The tissue was washed with PBS and immersed in graded sucrose series; it was then removed from the sucrose solution, submerged in a drop of Tissue-Tek O.C.T. Compound (Miles Scientific, Naperville, IL), and embedded in frozen O.C.T. Compound by using liquid nitrogen. The frozen block containing the tissue was cut into 10-μm sections

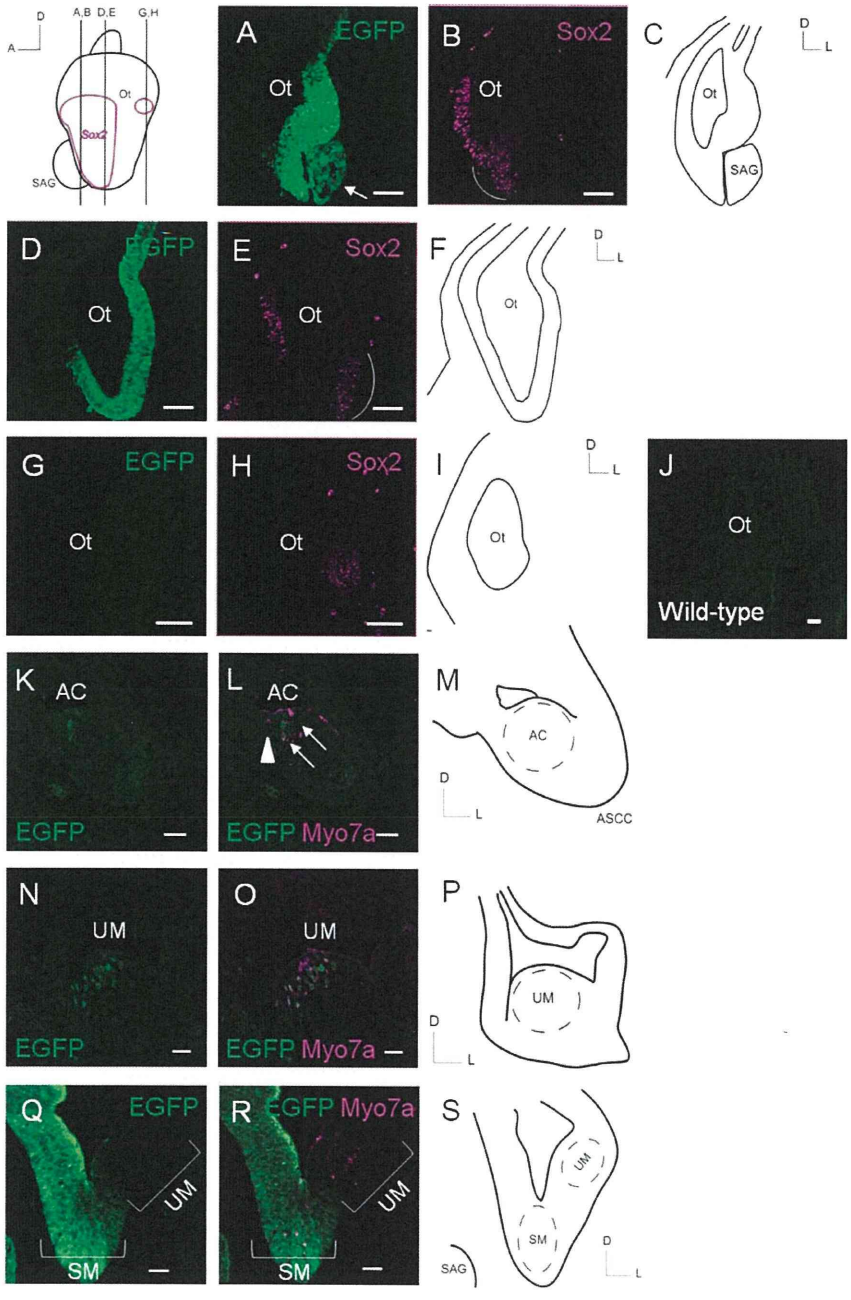

Figure 1 (legend on page 4707)

in the cryostat at 22–24°C and loaded onto freshly gelatinized slides.

The detailed method for construction of *Ednra*-lacZ knock-in mice has been described previously (Sato et al., 2008). *lacZ* expression was detected by staining with X-gal (5-bromo-4-chloro-3-indoyl β-D-galactoside) for β-galactosidase activity. Samples were embedded in the O.C.T. Compound, cryosectioned, and subjected to X-gal staining. Some sections were counterstained with 1% Orange G (Sigma-Aldrich, Milwaukee, WI).

FACS experiments

E10.5 otocyst epithelial cells samples were prepared for FACS experiments as follows. Otocysts were carefully dissected from freshly dissociated embryos of heterozygous *Ednra-EGFP* Line-14 transgenic and wild-type mice. Dissected otocysts were washed with PBS and then dissociated to a single-cell suspension by trypsin treatment for 10 minutes (200 μ; of 0.25% trypsin/ethylenediamine tetraactic acid solution). Then 1 ml of Dulbecco's modified Eagle's medium and 10% fetal calf serum (FCS) was added to the single-cell suspension. After centrifugation, the cells were resuspended in 0.5 ml of PBS and 5% FCS. Propidium iodide (PI) was added to a final concentration of 1 μg/ml.

FACS experiments were conducted on a FACSVantage SE (Becton Dickinson, San Jose, CA) equipped with a 488-nm argon laser. Emission filters were 530 ± 15 nm for GFP and 585 ± 21 nm for PI. The machine was flushed, and light-scattering parameters were calibrated with 2-μm beads. The rate of sorting was 200–1,000 cells/second through a 70-μm nozzle. Analysis was performed by using CellQuest software (Becton Dickinson).

The parameters for setting the EGFP-positive gate were established as follows. Cells were gated on the basis of light-scattering parameters (size, forward-scattered light; and granularity, side-scattered light) to exclude cellular debris as well as clumps of cells that may give erroneous fluorescent readings. Only cells that fell within the defined gate in the light-scatter plot were subsequently analyzed for fluorescent expression. Wild-type non-GFP cells were used to identify the population of autofluorescent cells. These scatter plots were compared with cell profiles from transgenic mice to define the EGFP sorting window. Nonviable cells were excluded by PI staining. Otocyst epithelial cells from heterozygous Line-14 embryos were sorted into EGFP-positive and EGFP-negative cells.

RNA extraction

Homogenization of cell lysates was performed by using QIAshredder homogenizers (QIAGEN, Hilden, Germany). Total RNA was extracted by using the RNeasy Plus Mini Kit (QIAGEN) according to the manufacturer's protocol. RNA quality was established by gel electrophoresis.

Microarray labeling, hybridization, and data processing

Ninety-six embryos (192 otocysts) from 12 heterozygous Line-14 embryos were used for the FACS experiments. Total RNA (1 μg) was extracted from the EGFP-positive and EGFP-negative otocyst epithelial cell samples at E10.5 sorted by FACS and used to synthesize biotin-labeled cRNA, which was then hybridized to a high-

Figure 1. EGFP expression in the developing inner ear and the statoacoustic ganglion of Line-14 and wild-type mice at E10.5 (A–J) and of Line-14 mice at E12.5 (K–S).**A–C:** A section from the anterior part of the E10.5 otocyst in Line-14 mice (A,B) and a schematic view of A (C). EGFP expression (green) was detected in the ventral and dorsomedial region of the otocyst and SAG neuroblasts (arrow in A). *Sox2* expression (magenta) was detected in the ventral and dorsolateral otocyst. In the EGFP-positive region in the ventral otocyst, *Sox2* expression was also observed (round bracket in B). In the *Sox2*-positive region in the lateral part, EGFP expression was not observed. In the EGFP-positive region in the dorsomedial part, *Sox2* expression was not observed. **D–F:** A section from the middle part of the otocyst in Line-14 mice (D,E) and a schematic view of D (F). EGFP expression (green) was detected in the ventral and dorsomedial regions of the otocyst. *Sox2* expression (magenta) was detected in the ventromedial and lateral otocyst. In the EGFP-positive region in the ventromedial otocyst, *Sox2* expression was also observed (round bracket in E). In the *Sox2*-positive region in the lateral part, EGFP expression was not observed. In the EGFP-positive region in the dorsomedial part, *Sox2* expression was not observed. **G–I:** A section from the posterior part of the otocyst in Line-14 mice (G,H) and a schematic view of G (I). *Sox2* expression (magenta), but not EGFP expression, was detected. **J:** A section from the otocyst in wild-type mice. No EGFP expression was detected. **K–M:** A section from the E12.5 anterior SCC (ASCC) in Line-14 mice (K,L) and its schematic view (M). EGFP expression was detected in some ASCC hair cells, which was confirmed by double staining with GFP (green) and Myo7a (magenta) (arrow in L). However, EGFP expression was not detected in the other ASCC hair cells (arrowhead in L). **N–P:** A section from the region in the E12.5 utricle apart from the saccule in Line-14 mice (N,O) and its schematic view (P). EGFP expression was detected in the utricular hair cells, which was confirmed by double staining with GFP (green) and Myo7a (magenta). **Q–S:** A section from the E12.5 utricle and saccule in Line-14 mice (Q,R) and its schematic view (S). EGFP expression was detected in the saccule including hair cells, which was confirmed by double staining with GFP (green) and Myo7a (magenta). However, EGFP expression was not detected in the utricle located adjacent to the saccule. See Supporting Information Figure S1 for EGFP expression patterns in other regions of the inner ear. Ot, otocyst; SAG, statoacoustic ganglion; AC, anterior crista; ASCC, anterior semicircular canal; UM, utricular macula; SM, saccular macula; A, anterior; D, dorsal; L, lateral. Scale bar = 50 μm (A,B,D,E,G,H,J), 20 μm (K,L,N,O,Q,R).

density oligonucleotide array (GeneChip Mouse Genome 430 2.0 array; Affymetrix, Santa Clara, CA). The sample preparation protocol from the Affymetrix GeneChip Expression Analysis Manual was used. The array contains approximately 45,000 probes interrogating ~34,000 mouse genes from UniGene (Build 107). After the arrays were washed, they were stained with streptavidin-phycoerythrin, and image data were collected and analyzed with an Affymetrix GeneChip Scanner 3000 (Affymetrix). Microarray Suite software 5.0 (Affymetrix) was used to calculate the average difference for each gene probe set, which is shown as the gene expression intensity value. The signal intensities were normalized so that the average for all genes on a GeneChip would be 100.

Evaluation of the prediction performance of the gene expression profile

To evaluate the capability of the gene expression profile in the GFP-positive region for predicting genes that are expressed mainly in the ventral and/or dorsomedial otocyst, we aimed to examine the conformity of the genes enriched in GFP-positive cells with the genes expressed mainly in the ventral and/or dorsomedial otocyst by using previously reported in situ hybridization data. We used the Gene Expression Literature Query Form and Gene Expression Data Query Form, both of which were established by the Gene Expression Database (GXD) project in The Jackson Laboratory (Bar Harbor, ME) and are accessible through the Mouse Genome Informatics website (Smith et al., 2007). In the Gene Expression Literature Query Form, the assay type, age, and abstract were set to in situ RNA (section or whole); E10.5; and the words "ear," "otic," or "otocyst," respectively. We searched the regional pattern of gene expression in the E10.5 otocyst, determined by in situ hybridization in all of the retrieved literatures. In the Gene Expression Data Query Form, the anatomical structure, developmental stage, and assay type were set to the words "ear," "otic," or "otocyst"; E10.0–11.25; and RNA in situ, respectively.

We searched the regional pattern of gene expression in the E10.5 otocyst by in situ hybridization for all the retrieved genes. All acquired genes that were expressed in the E10.5 otocyst from these two databases were categorized into the following three groups after the exclusion of some genes whose data did not exist in the microarray: Group 1, genes mainly expressed in the ventral and/or dorsomedial otocyst (i.e., the GFP-positive region in Line-14); Group 2, genes wholly expressed in the otocyst, genes whose expression was revealed not only in the ventral and/or dorsomedial otocyst but also in other parts of the otocyst, or genes whose expression was described in the literature without any in situ hybridization data; and Group 3, genes expressed in the otocyst but to a lower degree in the ventral and dorsomedial regions.

We evaluated the performance of the signal log ratio (SLR) for the forecast of genes expressed mainly in the ventral and/or dorsomedial otocyst. The outcome was defined as whether the gene belonged to Group 1. For the SLR of microarray data, we constructed a receiver operating characteristic (ROC) curve, in which the ordinate was sensitivity, and the abscissa was [1 − specificity]. At each cutoff value, sensitivity and specificity were calculated. The diagonal line corresponds to random forecasts, and the degree of concavity is considered as a measure of performance. The area under the ROC curve (AUC) was then calculated. An AUC value of 0.5 reflects random forecasts, whereas an AUC value of 1 implies perfect forecasts. Statistical analyses were conducted by using SPSS version 11.0J.

We set the optimal cutoff value of the SLR considering these statistical analyses. Then we defined the criteria for highly expressed genes in EGFP-positive cells, including a criterion involving the SLR.

Gene ontology analysis

To further characterize the sets of functionally related genes expressed in GFP-positive cells, we used the OntoExpress software (Intelligent Systems and Bioinformatics Laboratory, Detroit, MI) (Draghici et al., 2003) to classify genes according to the following gene ontology (GO) categories (Ashburner et al., 2000): biological processes and cellular components. GO terms overrepresented in our set of genes were identified by a hypergeometric distribution test controlled at a Benjamini-Hochberg false discovery rate of 5% (Benjamini and Hochberg, 1995).

Reverse transcription PCR

Reverse transcription (RT) was performed by using the QuantiTect Reverse Transcription Kit (QIAGEN) according to the manufacturer's protocol. For each PCR experiment, a negative PCR control (no cDNA template) was also conducted. Quantitative real-time RT-PCR was performed for *EGFP* and *Gapdh* with the LightCycler system (Roche Applied Science, Mannheim, Germany) according to the manufacturer's protocol. Sequences of specific primers used for *EGFP* and *Gapdh* used for real-time RT-PCR are shown in Supporting Information Table S1. Each cycle consisted of 15 seconds of denaturation at 95°C, 15 seconds of annealing at 65°C, and 8 seconds of extension at 72°C. Conventional RT-PCR was also performed for EGFP, glyceraldehyde-3-phosphate dehydrogenase (*Gapdh*), orthodenticle homolog 1 (*Drosophila*) (*Otx1*), orthodenticle homolog 2 (Drosophila) (*Otx2*), proline rich 15 (*Prr15*), gastrulation brain homeobox 2 (*Gbx2*), paired related homeobox 2 (*Prrx2*), ISL1 transcription factor

LIM/homeodomain (*Isl1*), bone morphogenetic protein 4 (*Bmp4*), jagged 1 (*Jag1*), lunatic fringe (*Lfng*), neurogenin 1 (*Neurog1*), *Sox2*, espin (*Espn*), *Myo7a*, eyes absent 4 homolog (Drosophila) (*Eya4*), eyes absent 1 homolog (Drosophila) (*Eya1*), GATA-binding protein 3 (*Gata3*), leukocyte cell-derived chemotaxin 1 (*Lect1*), and tumor necrosis factor receptor superfamily, member 12a (*Tnfrsf12a*).

The same primer sets for *EGFP* and *Gapdh* used for real-time RT-PCR were also used for conventional RT-PCR. Sequences of the other specific primers used are shown in Supporting Information Table S1. Conventional RT-PCR cycles consisted of 30 seconds of denaturation at 95°C, 30 seconds of annealing at 65°C (*EGFP* and *Gapdh*), 60°C; (*Espn*, *Myo7a*, *Eya4*, *Eya1* and *Gata3*), 59°C (*Lfng* and *Sox2*), 58°C (*Bmp4*, *Jag1*, and *Neurog1*), 56°C (*Otx1*, *Otx2*, and *Isl1*), and 55°C (*Lect1*, *Prr15*, and *Tnfrsf12a*); and 60 seconds of extension at 72°C.

RESULTS

One of the Ednra-EGFP transgenic mouse lines exhibited ectopic EGFP expression in the developing inner ear

We have established several *Ednra-EGFP* transgenic mouse lines with the *Ednra-EGFP* transgene. These mice shared EGFP expression in *Ednra*-expressing neural crest-derived ectomesenchyme (Fig. 2A), as observed in *Ednra-lacZ* knock-in mice (Sato et al., 2008), which exhibited *lacZ*-positive cells only in the dorsolateral otocyst (Fig. 2B). However, only one transgenic line, named *Tg(ETAR-EGFP)14Imeg* (Line-14), exhibited ectopic EGFP expression in the developing inner ear.

EGFP expression was first detected at E8.5–9.0 in the otic placode (Fig. 2C). At E10.5, EGFP expression was detected in the ventral and dorsomedial region of the otocyst (Figs. 1A–I, 2D). We observed the delamination of EGFP-positive neural-fated cells from the otic epithelium to the formation of SAG neurons (Fig. 1A,B). *Sox2* is considered to be a marker of the proneural/prosensory region of the otocyst that could be associated with presumptive cristae, utricular/saccular macula, organ of Corti, and SAG (Bok et al., 2007; Mak et al., 2009; Puligilla et al., 2010). Double-fluorescence immunohistochemistry of Line-14 revealed that both *Sox2* and EGFP were expressed in the ventral region of the otocyst (Fig. 1A,B,D,E). The dorsomedial region was positive for EGFP expression and negative for *Sox2* expression (Fig. 1A,B,D,E). In the anterior/posterior dorsolateral regions, some areas did not show EGFP expression but showed *Sox2* expression (Fig. 1A,B,D,E,G,H). EGFP was expressed in the ventromedial region, which could be destined to form the pars inferior; these results imply that the EGFP-positive region included a presensory domain of the pars inferior. They also indicated that EGFP would be partially expressed in the prosensory domain of the pars superior

When the otocyst differentiated into the labyrinth, which included both auditory and vestibular sensory patches, EGFP expression was detected in the cochlea, saccule, and endolymphatic duct (Fig. 2E,F). The EGFP-positive region in the pars inferior (the cochlea and saccule) included *Myo7a*-positive hair cells (Figs. 1Q–S, 3D–H). In the cochlea, the EGFP signals in the greater epithelial ridge were stronger than those in the lesser epithelial ridge (Fig. 3G,H). In the pars inferior, this line retained the spatiotemporal continuity of EGFP expression from the otocyst to sensory hair cells. Additionally, apart from the continuing EGFP-positive region, EGFP-positive cells were located in each semicircular canal (SCC) and the utricle (Figs. 1K–P, 3A–C). At E12.5, *Myo7a*-positive vestibular hair cells appeared, some of which were weakly EGFP-positive (Fig. 1K–S). At E13.5, all of the EGFP-positive cells in the SCCs and utricle became *Myo7a*-positive (Fig. 3A–C). In the sensory hair cells of the pars superior (the SCCs and the utricle), the spatiotemporal continuity of EGFP expression from the otocyst was not detected. Thus, these hair cells were likely to express EGFP from a certain stage of differentiation. As the differentiation into inner ear sensory patches progressed, EGFP expression was restricted to hair cells and some supporting cells (Fig. 3I–N) in the sensory patches and gradually diminished with the advance of morphological maturity (Fig. 3O,P). In adulthood, no EGFP expression in the inner ear was detected (data not shown).

The integration site of the transgene in Line-14 was at the intronic regions of the multiple C2 domains transmembrane 1 (Mctp1) gene

To clarify the mechanism underlying ectopic EGFP expression, we attempted to characterize the integration site of the transgene in Line-14. We extracted genomic DNA from Line-14 and Line-1 homozygous mice. Samples were digested with *Eco*RI, electrophoresed in an agarose gel, transferred to a nylon membrane, and hybridized with the ^{32}P-labeled EGFP fragment as a probe. Although the probe hybridized to a ban of ~1.1 kb, indicative of the tandem insertion of the transgene in *Eco*RI-digested DNA from mice of both lines, DNA derived from Line-14 showed an additional ~2.8-kb band (Fig. 4A). The ~2.8-kb band was considered to encompass the genomic DNA/transgene transition in Line-14.

By using the genome walking method, we identified the mouse genomic sequence flanking the 5′-end of the

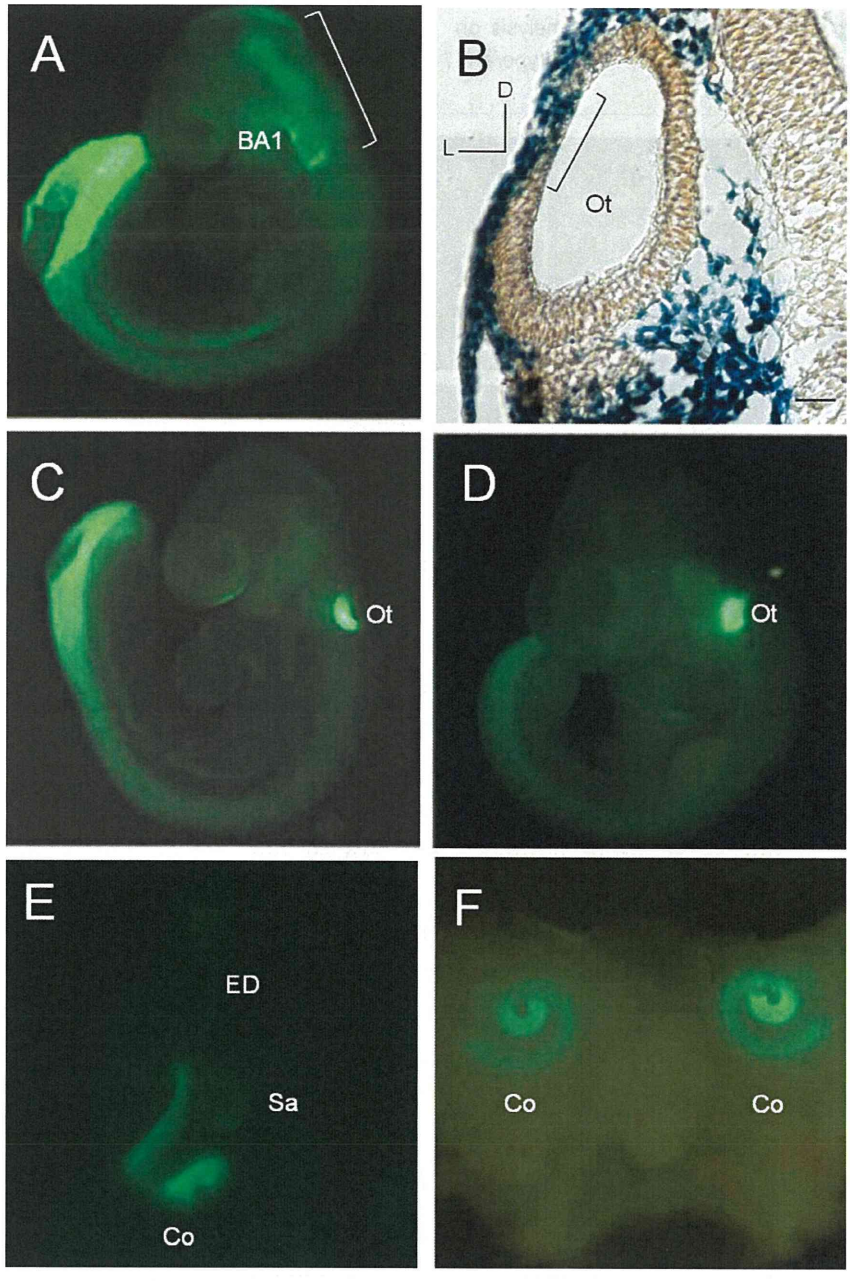

Figure 2. EGFP expressions in *Ednra*-EGFP transgenic lines. **A:** E9.0 embryo of *Ednra*-EGFP transgenic lines except Line-14. EGFP was mainly expressed in the neural crest-derived ectomesenchyme (bracket), where *Ednra* was originally expressed. **B:** E10.0 *Ednra-lacZ* knock-in mice exhibited lacZ-positive cells only in the dorsolateral otocyst (bracket). **C–F:** EGFP expression in the developing inner ear of *Ednra-EGFP* Line-14 transgenic mice. At E9.0 (C), EGFP expression was detected in the otic placode. At E10.5 (D), EGFP expression was detected mainly in the ventral and dorsomedial regions of the otocyst. At E14.5 (E), EGFP expression was detected mainly in the cochlea, saccule, and endolymphatic duct. F shows EGFP expression in the cochlear duct at E15.5. BA1, first branchial arch; Ot, otocyst; ED, endolymphatic duct; Sa, saccule; Co, cochlea; D, dorsal; L, lateral. Scale bar = 20 μm in B (applies to A–F).

transgene. BLAST search analysis revealed 100% identity with the 15th intronic sequence of the multiple C2 domains transmembrane 1 (*Mctp1*) gene (NCBI GeneID: 78771; Fig. 4B). Disruption of the intronic sequence by transgene insertion was confirmed by the absence of genomic PCR products with primers straddling the junction. Southern blot analysis of wild-type and transgenic genomic DNA with probes derived from the transgene showed patterns consistent with this integration (data not shown).

To examine the effect of transgenic insertion on the expression of *Mctp1*, we performed RT-PCR analysis on RNA samples extracted from the livers of wild-type and homozygous transgenic mice. Exon boundaries between exons 15 and 16 and adjacent sequences were intact in transgenic mice (data not shown), indicating that

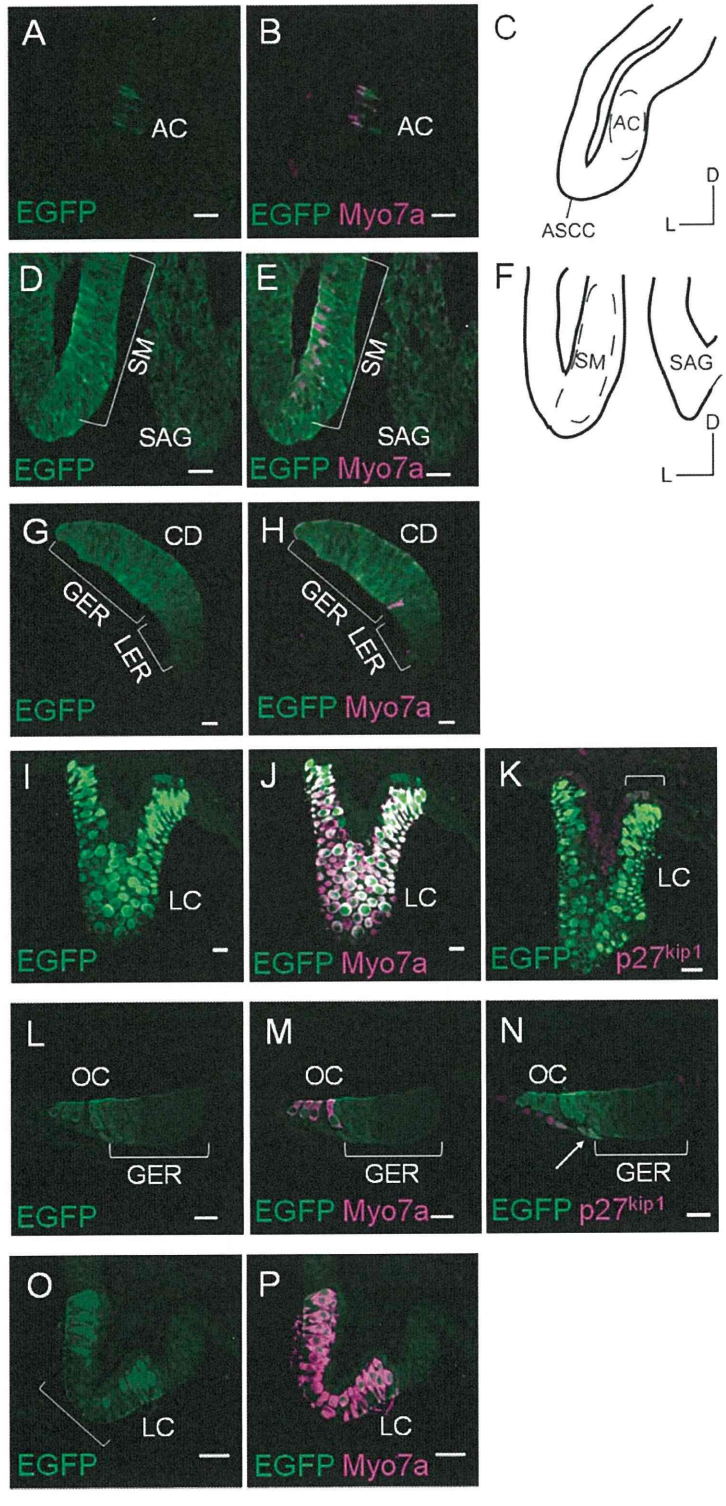

Figure 3 (legend on page 4712)